

# **A Multi-Modal Sweat Sensing Patch for Cross-Verification of Sweat Rate, Total Ionic Charge, and Na<sup>+</sup> Concentration**

*Zhen Yuan<sup>123#</sup>, Lei Hou<sup>123#</sup>, Mallika Bariya<sup>123#</sup>, Hnin Yin Yin Nyein<sup>123</sup>, Li-Chia Tai<sup>123</sup>, Wenbo Ji<sup>123</sup>,  
Lu Li<sup>123</sup>, Ali Javey<sup>123</sup>*

<sup>1</sup>Department of Electrical Engineering and Computer Sciences, University of California, Berkeley,  
California 94720, USA.

<sup>2</sup>Berkeley Sensor and Actuator Center, University of California, Berkeley, California 94720, USA.

<sup>3</sup>Materials Sciences Division, Lawrence Berkeley National Laboratory, Berkeley, California  
94720, USA.

#These authors contributed equally.

This file contains:

Supplementary Information Figure S1-S13.

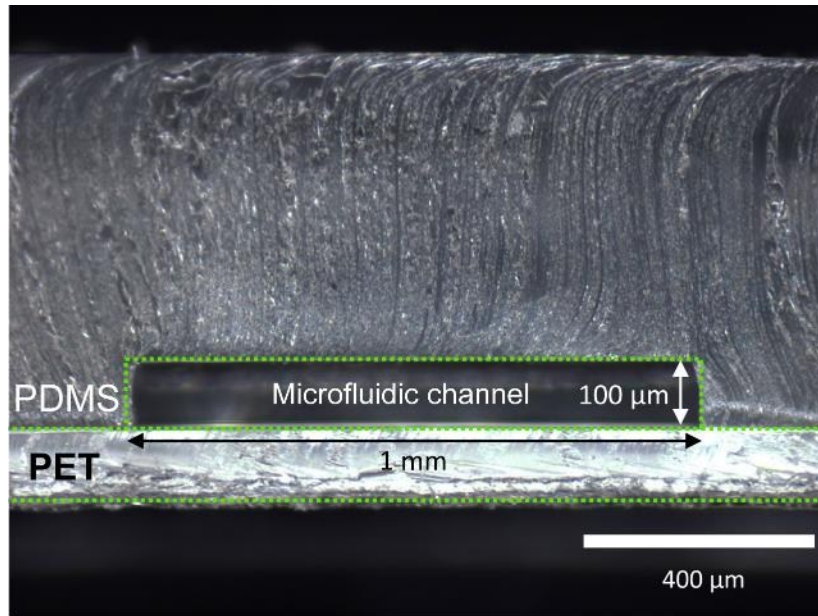


**Figure S1.** Optical microscope image of cross-section through PDMS microfluidic channel bonded to PET substrate.

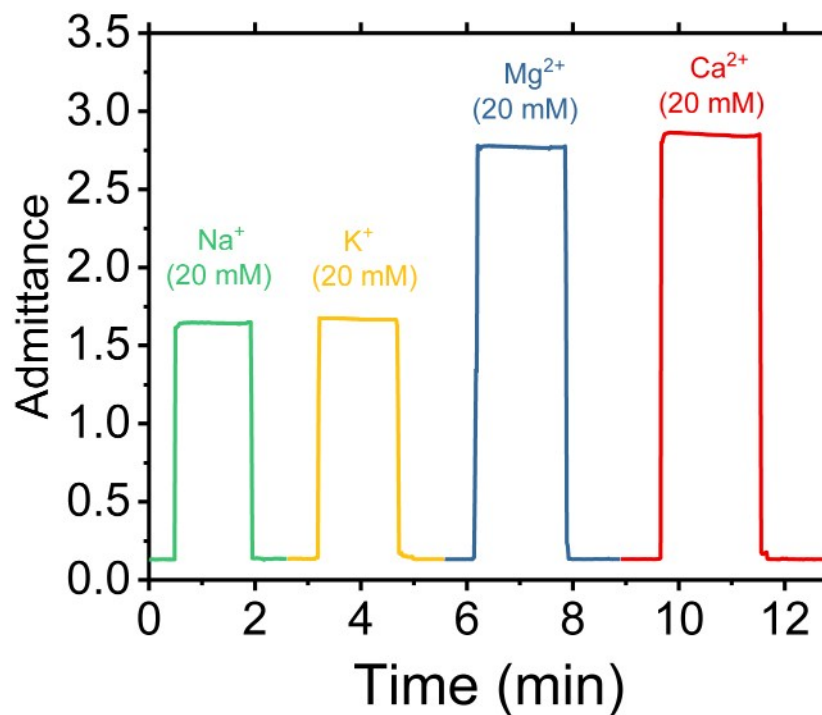


**Figure S2.** Response of total ionic charge sensor towards 20 mM of electrolyte species present in sweat. Sensor's admittance response depends on ion charge but is invariant to the specific species. Note that equal concentrations of Cl<sup>-</sup> are present in each test sample along with the cation concentrations listed above, but in general when converting the admittance signal back into ionic concentration, only cation concentration is indicated in this work.

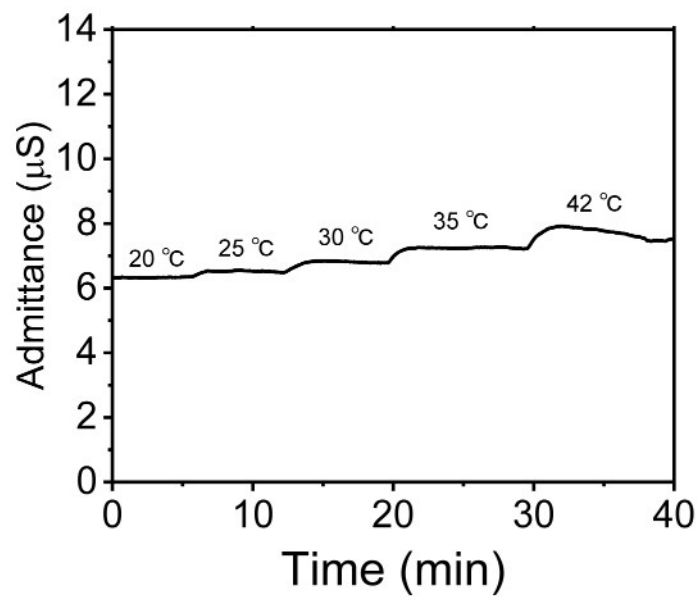


**Figure S3.** Thermal stability of sweat rate sensor admittance response to 100 mM NaCl at different temperatures.

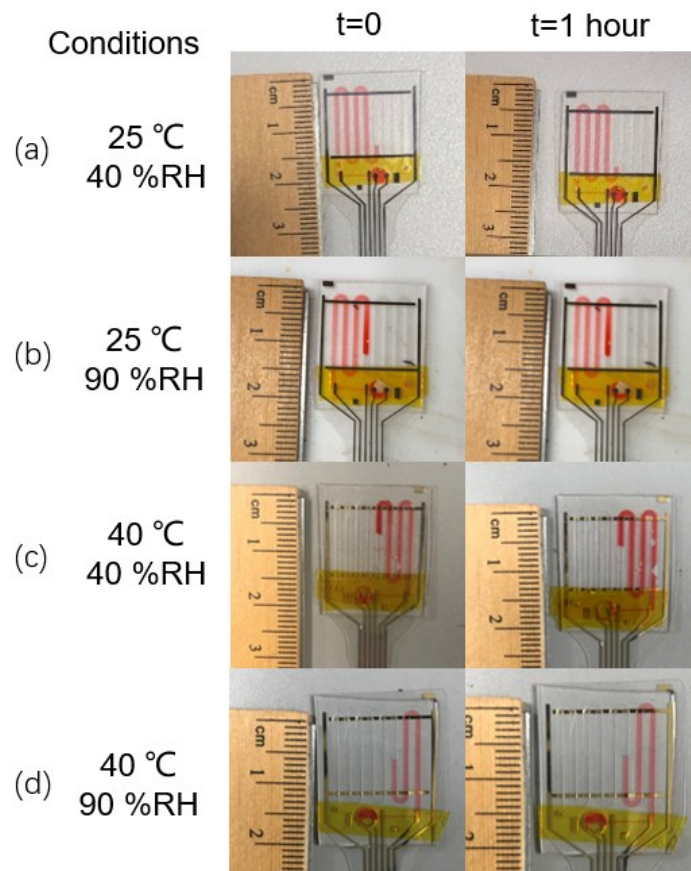


**Figure S4.** Evaporation of fluid in the microfluidic channel is assessed over 1 hr at different temperatures and relative humidities. Shifting of the red-dyed fluid front is considered to determine the degree of evaporation. Fluid loss is negligible at higher humidity levels across temperatures, and below 0.1  $\mu\text{l/hr}$  at lower humidity levels.

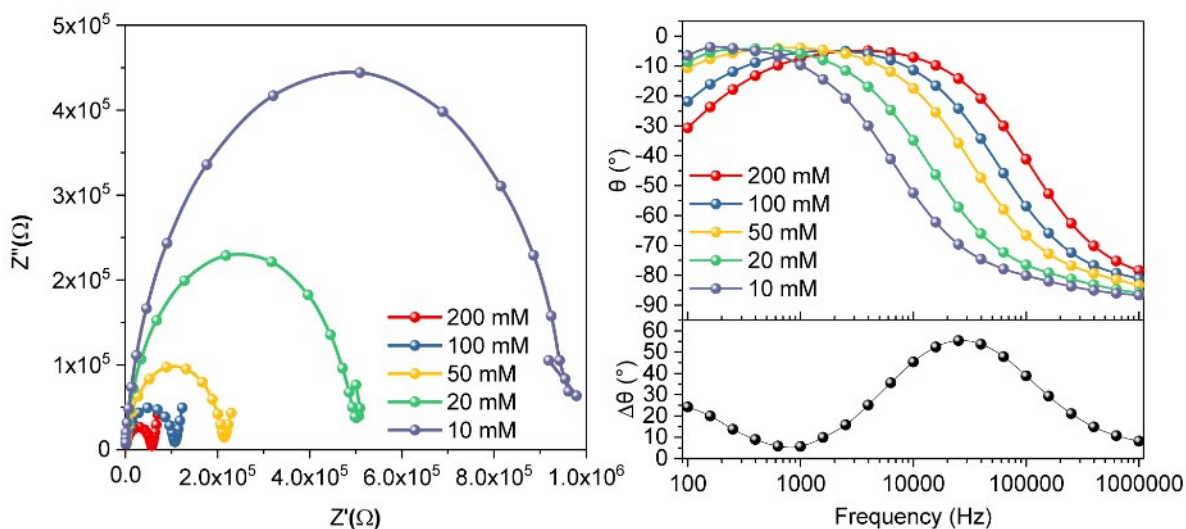


**Figure S5.** (a) Electrochemical impedance spectroscopy (EIS) Nyquist plot of sweat rate sensor in different concentrations of NaCl solution between 100 Hz and 1 MHz. (b) Corresponding Bode phase plot shows impedance phasor has similar angle  $\theta$  (within  $5^\circ$  variation given by  $\Delta\theta$ ) across the ion concentration range at 1 kHz, indicating the sweat rate sensor behaves as a linear system at this frequency with respect to fluid volumes of different concentrations. Sweat rate sensor admittance magnitude contributions of different segments/concentrations of fluid within the microfluidic channel can thus be added as scalars.

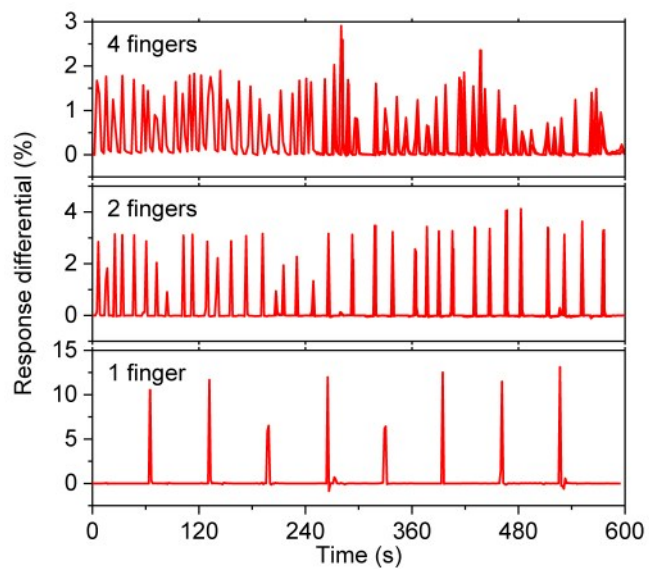


**Figure S6.** Differential signal from sweat rate sensors with 1, 2, and 4 interdigitated electrode fingers in response to 50 mM NaCl solution injected at 4.8  $\mu\text{L}/\text{min}$ . Number of fingers can be customized to optimize between signal-to-noise and temporal resolution when identifying admittance jumps for sweat rate estimation.

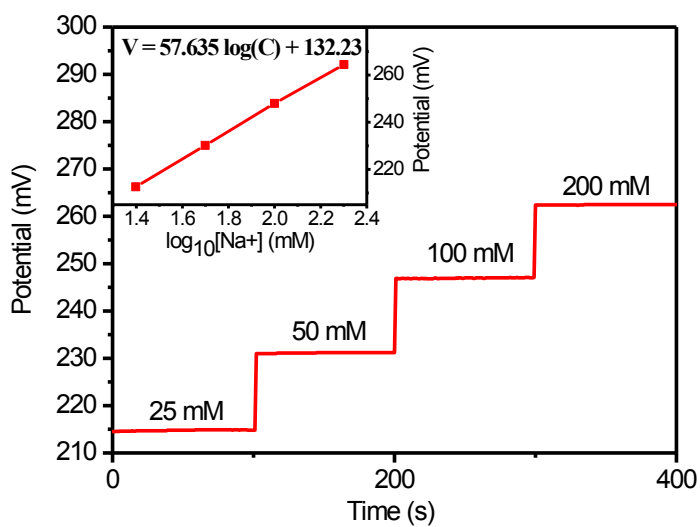


**Figure S7.** Calibration of a representative Na<sup>+</sup> sensor in 25 to 200 mM NaCl solution shows that the sensor response is linear over the entire range of concentrations detected during on-body trials.

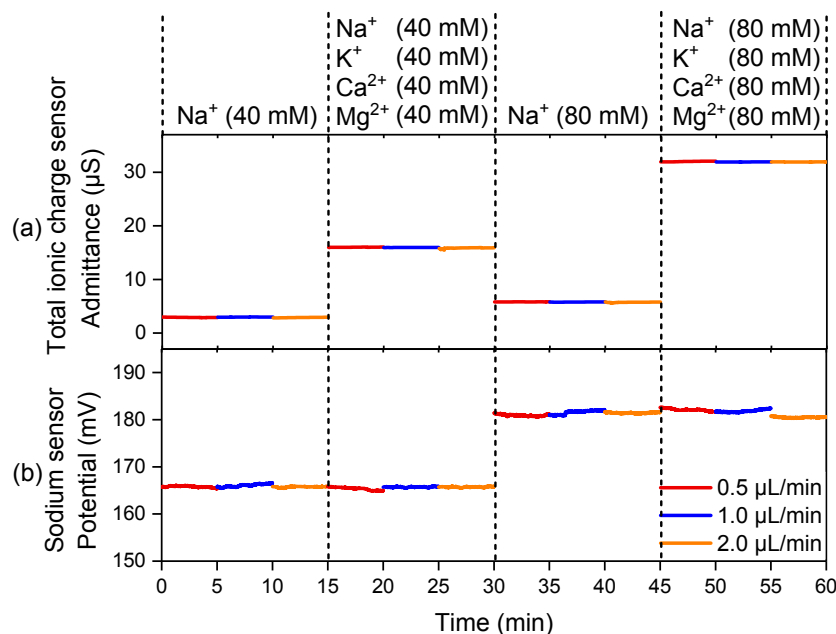


**Figure S8:** Total ionic sensor and sodium sensor responses to flow rate and ion concentrations.

(a) The total ionic sensor shows negligible dependence on flow rate, responding selectively to changes in total ionic concentration upon addition of  $\text{Na}^+$ ,  $\text{K}^+$ ,  $\text{Mg}^{2+}$ , or  $\text{Ca}^{2+}$  ions. (b) The  $\text{Na}^+$  sensor shows no significant response to changing flow rate or the addition of  $\text{K}^+$ ,  $\text{Mg}^{2+}$ , or  $\text{Ca}^{2+}$  interfering ions but responds sensitively to changes in  $\text{Na}^+$ .

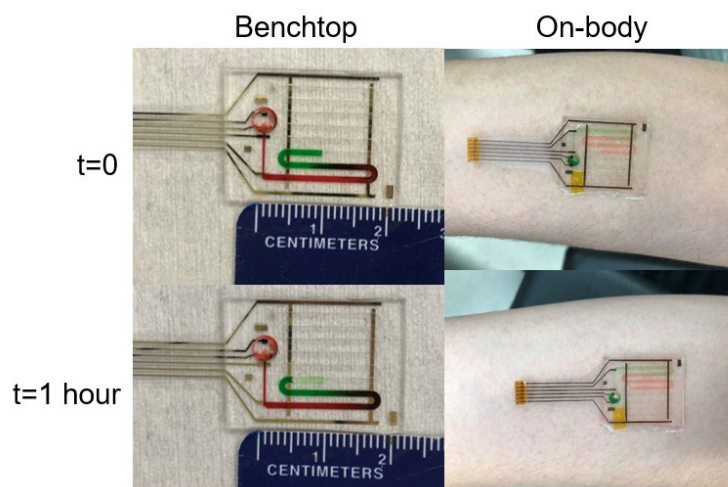


**Figure S9.** Testing convective fluid mixing within the microfluidic channel. Photo images depict the sensor with sequentially injected portions of red and green-colored fluid. The images are taken before and 1 hr after the fluid is injected, while the sensor sits at rest on the benchtop or is attached to the forearm during exercise. Minimal change in the interface between segments of differently dyed fluid indicate that mixing is low.

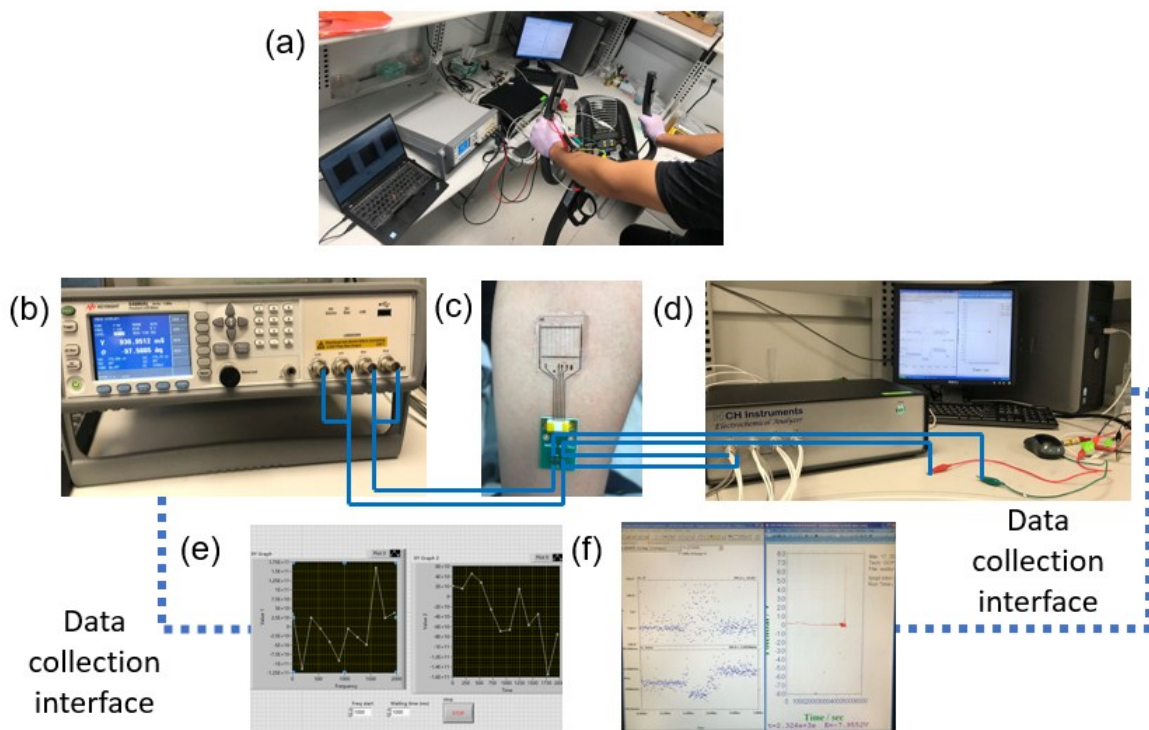


**Figure S10.** Instrument set-up used to capture sensor readings in real-time during on-body measurement. (a) The complete experimental set-up and instrument connections during stationary biking exercise, showing (b) LCR meter for sweat rate sensor, (c) on-body microfluidic patch with connector board to instruments, (d) Gamry and CHI 1430 potentiostats for the total ionic sensor and  $\text{Na}^+$  sensor respectively, (e) data collection interface for the LCR meter, (f) data collection interfaces of Gamry and CHI 1430.

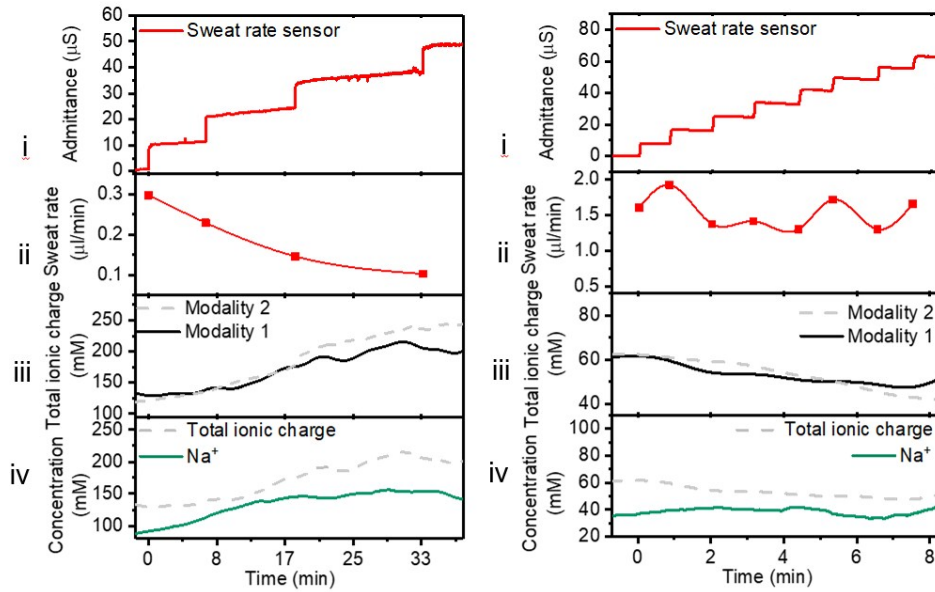


**Figure S11.** Trials 5 and 6 showing real-time, on-body sweat analysis during stationary biking exercise, with simultaneous measurement of (i) raw sweat rate sensor admittance data, (ii) sweat rate, (iii) total ionic charge concentration, and (iv)  $\text{Na}^+$  concentration profiles. Trial 5 is obtained from Subject A and Trial 6 from Subject C.

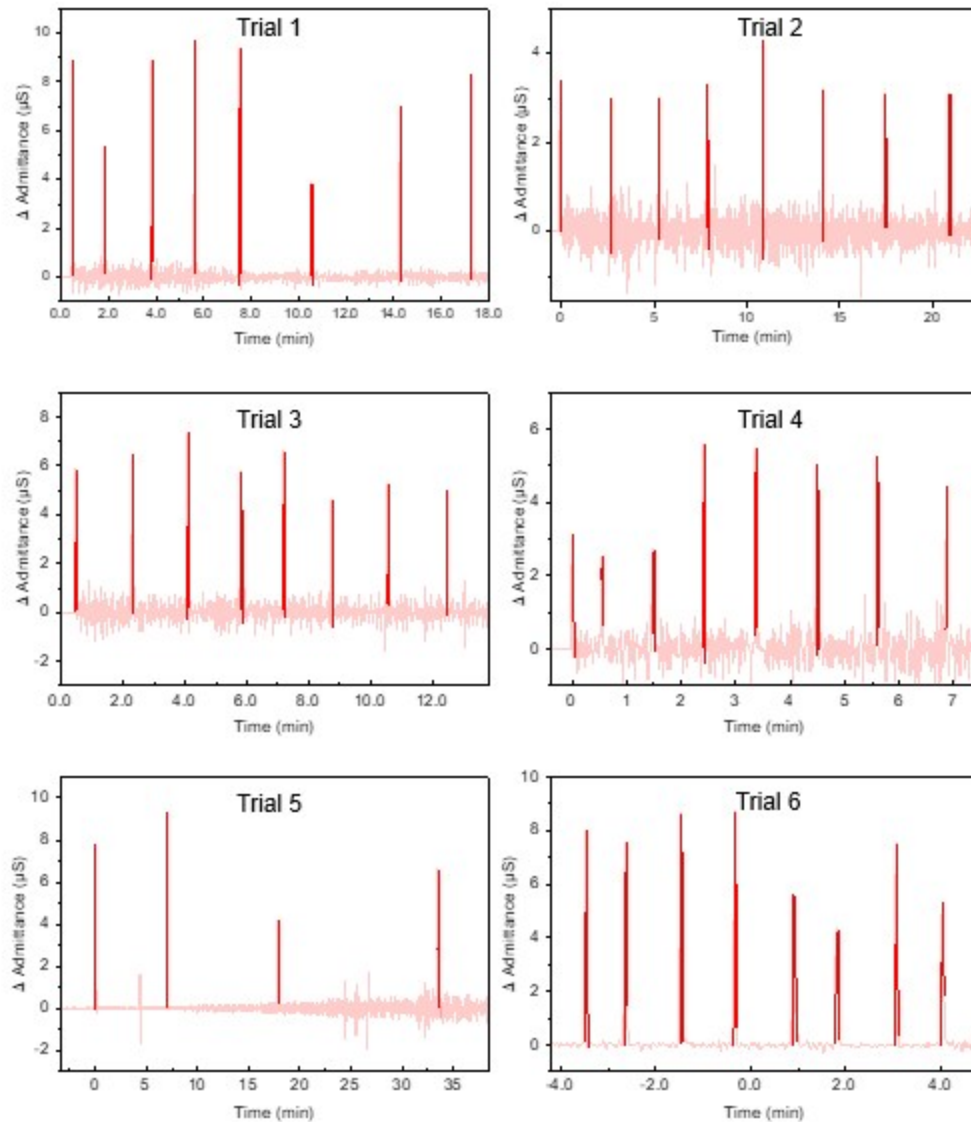


**Figure S12.** The differential signal of sweat rate sensor admittance signal for on-body sweat analysis Trials 1-4 from Fig. 6 and 5-6 from Fig. S11. These signals are used to reconstruct the sweat rate profiles in panels labeled ii in Fig. 6 and S11, and to estimate total ionic charge concentration via Modality 2, seen as dashed grey lines in panels labeled iii.

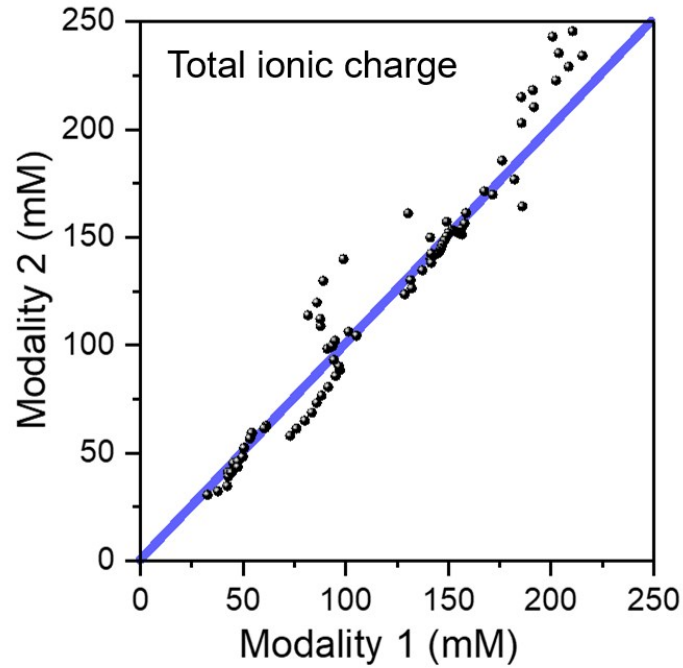


**Figure S13.** 1-to-1 comparison of Modality 1 (total ionic sensor) vs Modality 2 (sweat rate electrodes) for total ionic charge sensing. Black points represent sampled data from on-body Trials 1-6 (20 points sampled at regular intervals from each trial). The blue line of slope 1 is shown for comparison.